

July 1980

LRP 170/80

RESONANT ABSORPTION OF ALFVEN WAVES IN FAT
TORI WITH CIRCULAR CROSS-SECTION

K. Appert, B. Balet, R. Gruber, F. Troyon,

T. Tsunematsu and J. Vaclavik

RESONANT ABSORPTION OF ALFVEN WAVES IN FAT TORI WITH
CIRCULAR CROSS-SECTION

K. Appert, B. Balet, R. Gruber, F. Troyon, T. Tsunematsu^{*)}
and J. Vaclavik

Centre de Recherches en Physique des Plasmas
Association Euratom - Confédération Suisse
Ecole Polytechnique Fédérale de Lausanne
CH-1007 Lausanne / Switzerland

^{*)} on leave from JAERI, Tokai, Japan

ABSTRACT

The heating of toroidal plasmas by resonant absorption of Alfvén waves is considered in the framework of ideal MHD. We show that the overall picture of Alfvén wave heating in a fat torus does not fundamentally differ from that in a cylinder. The toroidal plasma may efficiently be heated internally when a collective mode is excited. The main toroidal effects are a shift of the resonant surface towards the plasma centre and an increased reactive power which shows up as enhanced motion near the plasma edge.

1. INTRODUCTION

Several years ago resonant absorption of Alfvén waves in non-uniform plasmas was proposed^{1,2} as a supplementary heating scheme for magnetically-confined fusion devices. Up to now the idea has been tested experimentally on pinch- and stellarator-like devices^{3,4,5} and it seems that energy may easily be deposited in the plasma by this method. It remains to be seen⁶ whether this method is applicable to tokamaks as well.

The basic ideal MHD theory for the rate of energy absorption using the Alfvén wave heating scheme has been given by Chen and Hasegawa⁷ using a simple slab geometry. They found that the absorption rate is strongly enhanced when the nonuniformity of the plasma equilibrium is sharp and the driving frequency is close to the frequency of the weakly-damped surface mode. Recently, we have shown⁸ that a similar phenomenon takes place in a cylindrically-symmetric equilibrium with an arbitrary nonuniformity. On the other hand it has frequently been conjectured that it might be impossible to heat the interior of toroidal plasmas with Alfvén waves. The concern was that the pump might more easily couple to resonant surfaces near the plasma edge than to those in the interior of the plasma. The question is whether or not the toroidicity may substantially modify the results obtained with the cylindrical models. In the present paper we investigate Alfvén wave heating of toroidal axisymmetric plasmas to answer this question. We use an ideal MHD model for our investigation which allows us to compute the plasma loading resistance and reactance.

The paper is structured as follows. In ch. 2 we present the equilibrium and the antenna structure used in our numerical model. Ch. 3 contains a short review of the physics relating to Alfvén wave heating. In ch. 4 we mention some numerical details and explain the limits of our computational model. In ch. 5 and ch. 6 we present the physical results concerning mode structures and energy absorption. Finally, we draw the main conclusion in ch. 7.

2. COMPUTATIONAL MODEL

For the sake of clarity, the unperturbed plasma is described by a simple one-parameter class of Solov'ev's equilibrium.^{9,10} The free parameter is R/a , the aspect ratio, where R and a denote the major and the mean minor radius of the torus respectively. The characteristic features of the chosen class of equilibria are the safety factor, $q_0 = 1$ on the axis, the toroidal magnetic field and current profiles of the form $B_T \propto 1/d$ and $j_T \propto d$ and nearly circular plasma cross-sections, d being the radial coordinate measured from the main axis of the torus. For an infinite aspect ratio j_T is constant within the plasma. Note that the toroidal field B_T is a vacuum field. In table 1 the safety factor on the plasma surface, q_s , and the mean total β are given for some values of the inverse aspect ratio, a/R .

Table 1

a/r	q_s	β {%
0.1	1.04	1.0
0.2	1.18	3.7
0.25	1.31	5.4
0.275	1.40	6.4
0.3	1.52	7.2
0.333	1.74	8.4

The mass density has a parabolic profile falling to 10% of the centre value at the plasma edge.

The Alfvén waves are excited by an ideal infinitely thin antenna which is located in the vacuum region between the plasma torus and a perfectly conducting shell. The cross-sections of the antenna and the shell form concentric circles around the magnetic axis of the plasma.

Their radii are $\rho_A = 1.6 a$ and $\rho_S = 2 a$ respectively. The spatial dependence of the surface current density flowing in the antenna is given by

$$\underline{J}_p = \frac{m a B_{T_0}}{2 \rho_A \mu_0} \left\{ I^S \sin m \theta \cos n \varphi - I^A \cos m \theta \sin n \varphi \right\} \quad (1)$$

together with the condition $\text{div } \underline{J} = 0$. Here m and n denote the poloidal and toroidal mode numbers of the antenna structure, θ and φ are the poloidal and toroidal angles, B_{T_0}/μ_0 is the intensity of the toroidal field on the magnetic axis and I^S and I^A are dimensionless currents. These are taken to be either $I^S = I^A = 1$ or $I^S = 1, I^A = 0$.

The first combination corresponds to an (m,n) - helical antenna structure with a total current per "wire" of $a B_{T_0}/\mu_0$. The latter describes the superposition of an (m,n) -, and a $(-m,n)$ - helical antenna with a current per "wire" of $a B_{T_0}/2\mu_0$. As for the currents all other quantities in this paper are given in dimensionless units. The units of length and time are a and R/c_{A_0} respectively, the Alfvén velocity (c_{A_0}) is evaluated on the magnetic axis and the absorbed power per unit length of the machine p scales with $a c_{A_0} B_{T_0}^2/\mu_0$.

The plasma motion is described by the standard ideal MHD equations

$$\rho \ddot{\underline{\xi}} = \underline{F}(\underline{\xi}) \quad (2)$$

supplemented by the appropriate boundary conditions. Modified versions of the Lausanne stability codes THALIA (1D)¹¹ and ERATO (2D)¹² have been used for their solution.

3. CONTINUOUS SPECTRUM AND RESONANT ABSORPTION

For the interpretation of our numerical results it is important to have a thorough understanding of the basic physics underlying Alfvén wave heating. We therefore review briefly the most important points.

The Fourier transform of eq.(2) is a linear eigenvalue problem

$$-\omega^2 \underline{f} = \underline{F}(\underline{f}). \quad (3)$$

There are 3 classes of eigensolutions to this equation: the fast and slow magnetoacoustic waves and the Alfvén waves. In nonuniform plasmas the Alfvén waves and the slow waves exhibit continuous spectra; there exists an eigenmode satisfying eq.(3) for every frequency in a certain range. These eigenmodes have the character of distributions in space. They are not square integrable, but their superposition yields integrable, physically meaningful functions.

To be specific let us consider Alfvén waves in a cylindrically-symmetric equilibrium. Eq.(3) may then be Fourier transformed with respect to θ (poloidal angle) and z . We therefore look for eigenmodes of the form $\exp[i(m\theta + kz)]$. We will find that to any frequency ω which meets the local Alfvén frequency $(B_\theta m/r + B_z k)/\sqrt{\rho\mu_0}$, on some point r_s , within the plasma, there exists an eigenmode which is singular at r_s . The class of the Alfvén modes constitutes an ensemble of infinitely many oscillators, continuously distributed in space and frequency.

Imagine now that such a system is to be excited with a given pump frequency ω_p within the range of the continuum, starting at time $t = 0$. Initially a broad band of frequencies is excited, but as time progresses the bandwidth tends towards zero and yet infinitely many modes remain in resonance with the pump and grow in amplitude. The system therefore, "absorbs" energy at a constant rate by increasing the energy content

of an ever diminishing thin layer around the resonant surface at r_s . Obviously, this is an unphysical answer. The inclusion of any physical dissipation mechanism, however small, will prevent the system from evolving so far. It will attain a stationary state where the dissipation in the neighbourhood of the resonant surface just balances the energy inflow from the pump. The important point now is that the absorbed energy depends on neither the specific dissipation mechanism nor its quantitative value. An analogous case is that of a damped harmonic oscillator being acted upon by a force with a continuous spectrum.¹³

There are two different ways to calculate numerically the "absorbed" power in the framework of ideal MHD. The first is to solve eq.(2) subject to the appropriate boundary conditions as an initial value problem. The spatially discretized problem then takes the form

$$\underline{\underline{B}} \cdot \ddot{\underline{x}} = \underline{\underline{A}} \cdot \underline{x} + \underline{\underline{S}} \sin \omega_p t \quad (4)$$

where \underline{x} is the discretized displacement, and $\underline{\underline{A}}$, $\underline{\underline{B}}$ and $\underline{\underline{S}}$ are the kinetic and the potential energy matrices and the pump vector. The second way of doing it is to add an artificial damping term to eq.(2) and asking for the stationary state behaving as $\exp(i\omega_p t)$. The equation to be solved then becomes,

$$(-\omega_p^2 + 2i\nu\omega_p) \underline{\underline{B}} \cdot \underline{x} = \underline{\underline{A}} \cdot \underline{x} + \underline{\underline{S}} \quad (5)$$

which is a linear algebraic equation for \underline{x} . This approach demands much less computer time than the one using eq.(4). It provides one however, with less physical insight into resonant absorption than the former.

For these reasons both approaches, eq.(4) and eq.(5), have been made in a 1D cylindrical model, but only eq.(5) has been used in 2D. Illustrative results from the 1D codes are given in Figs. 1 and 2. In Fig. 1 an evolutionary run is documented by the spatial profile of the poloidal displacement ξ_θ , at three subsequent times. The increasing concentration of energy around the resonant layer at $r_s = 0.5$ is evident. In the lower part of the picture the absorbed power, defined as the time average of the total power delivered by the antenna, is plotted versus time. The arrows indicate the times at which ξ_θ is shown. Most strikingly, after two pump periods $2\pi/\omega_p$, the value of p is already in the vicinity of the asymptotic value $p = .021$. The very low frequency transient at times $\omega_p t/2\pi < 30$ is a slow magnetoacoustic wave excited when switching on the pump. In Fig. 2 the spatial wave forms of $\text{Re } \xi_\theta$ are shown as produced with the stationary version of the code. Three different values of the artificial damping coefficient ν , have been used. The calculated absorbed powers agree within 10% with each other and with that obtained with the evolution code. All the oscillations far from the resonant surface are damped in this case.

There remains one important piece of physics to be mentioned: the collective plasma oscillations with frequencies in the continuum. Analogous to the Vlasov operator in velocity space whose Fourier picture yields a continuous spectrum associated with the distributional Van Kampen eigenmodes and whose Laplace picture yields the weakly-damped collective oscillations of Landau, the ideal MHD operator in configuration space has its distributional eigenmodes and its damped collective oscillations. In the case of interest here the collective mode is a remnant of the first fast wave which has disappeared in the continuum. It may reappear as a real eigenmode in the Fourier picture in either unstable situations (kink) or in equilibria with discontinuities (surface eigenmode).

4. LIMITS TO THE COMPUTATIONAL MODEL

The discretization in space imposes a fundamental restriction on the time to which the evolution code may be run and also a lower bound ν_{\min} , on the artificial damping rate ν , which is used in the stationary code. The discretization in space results in a discretization in frequency. Numerically the continuum is approximated by a discrete spectrum in which the frequencies are related to the local Alfvén frequencies on the radial mesh.

Therefore, to each mesh width there corresponds a frequency spacing $\Delta\omega$. A minimum constraint on t_{\max} or ν_{\min} may be obtained by requiring that the code should be unaware of the discreteness of the continuum as long as at least two frequencies are resonant with the pump. Hence

$$t \ll t_{\max} = 2\pi/\Delta\omega,$$

$$\nu > \nu_{\min} = \Delta\omega,$$

(6)

where $\Delta\omega$ has to be evaluated at the resonant surface.

To illustrate this we present in Fig. 3 the absorbed power versus a wide range of artificial damping rate ν , as determined with the 2D code. The equilibrium used had an inverse aspect ratio of $a/R = 0.275$, and in the following we will refer to this value as the TCA-value.⁶ The excitation was $m = \pm 1$, $n = 2$. Two pump frequencies have been chosen differing by $\Delta\omega/2$. The frequency $\omega_p = 3.58$ was equal to an eigenfrequency in the "continuum", the frequency $\omega_p = 3.61$ on the other hand lay in between two eigen-

frequencies. From Fig. 3 it can be seen that quite accurately for $\nu \gtrsim \nu_{\min} = \Delta\omega = 0.06$ the system does not feel distinct eigenvalues anymore and produces the same value of p for the two frequencies. Also p depends only very weakly on the value of $\nu \gg \nu_{\min}$: less than 20% variation of p when ν varies over an order of magnitude.

It is important to mention here that all our results are affected by some uncertainty related to the choice of ν . This becomes even clearer when inspecting the two-dimensional mode structures of the resonant Alfvén waves. In Fig. 4 we show the mode structures as obtained with $\nu = 0.03$ and $\nu = 0.3$ in the runs made for Fig. 3, $\omega_p = 3.58$. The plots represent the real part of the displacement $\underline{\xi} = (\xi_s, \xi_\chi)$ on the gridpoints of the nonorthogonal coordinate system s, χ as used in ERATO.¹² The coordinate s labels the surfaces of constant poloidal flux, and χ is the natural measure for the poloidal angle in a toroidal equilibrium. In the case of an infinite aspect ratio s and χ become r and θ respectively. The main axis of the torus lies to the left of the cross-sections shown in Fig. 4. The innermost excited surface is the $m = 1$ resonant surface followed by the $m = -1$ surface. Near the plasma edge higher m modes are excited by toroidal effects. These modes are barely to be seen in Fig. 4a but show up very clearly in Fig. 4b. The difference comes from the fact that the modes near the plasma edge have greater $\Delta\omega$ than the modes $m = 1$ and $m = -1$. Fig. 3 shows that $\nu = 0.03$ is an absolute minimum for the modes $m = \pm 1$. This value is definitely too small for the other modes to give a physically meaningful contribution to the overall absorbed power. They are appropriately treated with $\nu = 0.3$ (Fig. 4b). Here, we should pay attention to the fact that the absorbed power barely changes for $\nu > 0.03$ in Fig. 3. This is the first indication for our final finding that the modes near the plasma edge are badly coupled to the pump. They do, however, contribute to the reactive energy in the plasma as can be seen from the substantial displacements near the plasma edge.

For the choice of ν we now have to make some form of compromise. On the one hand we would like to have the artificial damping coefficient ν much smaller than the pump frequency such that the physical results are not affected. On the other hand higher surfaces could be missed if ν is not of the order of the pump frequency. This situation is met especially in equilibria with small mass density near the edge. In general these uncertainties may be assessed by varying the nonequidistant radial mesh and the value of ν . In this paper up to 80 radial and 30 azimuthal intervals have been used to discretize the upper half poloidal plane. The values of ν as well as the meshes have been varied in order to produce error bars on p (see e.g. Fig. 10).

5. MODE STRUCTURES

We now study the influence of toroidicity on the mode structures in detail. In a torus the toroidal field B_T varies to lowest approximation according to $1/(1 + a/R \cos \chi)$ on a magnetic surface. This cosine-dependence causes a linear coupling of $\cos(m\chi)$ - modes to modes with $\cos(\underline{m+1}\chi)$. This coupling is evidenced in Fig. 5. The mode structure resulting from an $(m=1, n=2)$ - excitation of the TCA-equilibrium has been Fourier-analyzed along χ . In Fig. 5 the radial dependence of the 5 dominant Fourier amplitudes of the poloidal displacement $\xi_{\chi}^{m,n}$, are shown in the vicinity of the $m = 1$ resonant surface. The ratio between neighbouring amplitudes is roughly given by a/R . In Fig. 6 the maximum amplitudes at the resonant surface are plotted versus a/R . They are normalized by $\xi_{\chi}^{1,2}$. The dashed lines indicate that the components $m \neq 1$ vanish for infinite aspect ratio. We conclude that the pure $m = 1$ angular dependence at the resonant surface $m = 1$ of a straight cylinder becomes a combination of different m -numbers in the case of a torus. Due to this fact an $m = 1$ pump may also excite modes at surfaces $m \neq 1$. This phenomenon is documented in the two following pictures.

In Fig. 7 we show the local Alfvén frequencies for the case of a straight cylinder corresponding to the TCA-equilibrium and $n = 5$:

$$\omega_A^2 = (n + m/q)^2 / \rho . \quad (7)$$

The correspondence between 1D and 2D quantities is given by

$$r = s , \quad k = n/R , \quad q = rB_z / (RB_0) . \quad (8)$$

We have chosen the case $n = 5$ for two reasons. Firstly, more surfaces $m \neq 1$ appear than in the previously discussed case $n = 2$; and secondly, the case $n = 5$ is particularly interesting with respect to power absorption as will be shown later. The arrows indicate where the surfaces r_s , for different m should lie given the pump frequency, $\omega_p = 6.73$.

In Fig. 8 we show some details of the mode structure for this excitation. In order to make the relation to Fig. 7 evident, we have copied the arrows from Fig. 7 to Fig. 8 using the correspondence, eq.(8), $s = r$. Only the dominant Fourier components are plotted versus s together with the $m = 1$ component. The complete picture would contain lower peaks of other m -numbers underneath every peak as has been shown in Fig. 5. There are two striking features in this mode structure. First of all there is a systematic shift of the 2D resonant surfaces s_r , towards the plasma centre as compared to their 1D location r_s . The appearance of $m = -5$ and $m = -6$ surfaces near the plasma edge is also due to this toroidal shift. Secondly, the surfaces $m = 0$ through -3 are not dominated by their intrinsic angular dependence but by a wave number decreased by one, i.e. $m = -1$ through -4 . The intrinsic dependence manifests itself in the increasing height of the wings situated to the right of the respective maxima as one goes from $m = -1$ to $m = -4$.

6. ENERGY ABSORPTION

Judging from the mode structures in Fig. 8, one tends to believe that toroidal effects play a dominant role in Alfvén wave heating. This is, however, not always the case as far as the absorbed power is concerned. In Fig. 9 we show results which seem at first sight to be paradoxical. They demonstrate that under certain conditions the 1D and the 2D models agree better with increasing inverse aspect ratio a/R . We show the absorbed power per unit length of the machine p , and the Q-value, i.e. the ratio of the reactive power to the absorbed power for an excitation $m = 1$ and $n = 2$. The pump frequency is chosen such that the resonant surface lies at $r_s = 0.5$ in the 1D model. The dominant physics of this picture, increasing p for increasing a/R , can be understood from the earlier 1D studies of Alfvén wave heating.^{2,7,8} As we have chosen $n = k R = 2$ in this run, the relevant 1D wave number $a k$ varies with a/R . In the 1D studies efficient absorption in the interior of the plasma has only been found when $a k$ and ω_p were near to the resonance condition for a collective mode. The parameters in Fig. 9 are such that we approach the resonance with a collective mode when increasing a/R . The error bars on the absorbed power indicate the fact that it is difficult to achieve good convergence with respect to v when the absorbed power is low. Within these error bars we do not detect any toroidal effect on the absorbed power. The reactive power on the other hand, is affected by the toroidicity. Astonishingly, this effect is greater for greater aspect ratio. For $a/R = 0.1$ the difference between 1D and 2D is due to the remaining toroidal shift which is of the order of 10%. For $a/R = 0.3$ the effect of the toroidal shift which is 20% here, is masked by the resonance with the collective mode.

In Fig. 10 we show the resonance with the collective mode explicitly by varying the wave number n for the TCA-equilibrium with an $m = 1$ antenna and a pump frequency chosen such that the 1D resonant surface lies on $r_s = 0.5$. In spite of the fact that the corresponding 2D resonant surface s_r , is shifted towards the plasma centre, the 1D and the 2D models produce practically the same results. This is one of the rare cases where toroidicity has a beneficial effect: Compared with a cylindrical plasma it is easier to heat the inner region of a toroidal plasma. On the other hand the tendency seen in Fig. 9 of a higher Q -value in the toroidal case is confirmed here. However, its numerical value at resonance $Q = 6$, is acceptable from the experimental point of view, where the requirement is that Q should be less than 10.

From Fig. 3, 9 and 10 we draw the conclusion that if a collective mode favours a certain surface, practically all the energy may be absorbed at that surface. Yet the results shown in the last picture, Fig. 11, question to a certain extent this firm conclusion. We show the absorbed power versus the pump frequency for TCA excited with $m = 1$, $n = 2$. The artificial damping coefficient was on the low side, i.e. $\nu \sim \Delta\omega$, where $\Delta\omega$ was evaluated at the resonant surface $m = 1$. The location of the resonant surfaces r_s (1D) and s_r (2D) are indicated for each run. We see that the agreement between 1D and 2D is perfect for surfaces lying well inside the plasma. For an excitation near to the plasma edge, however, the 2D model predicts absorbed powers which exceed the corresponding 1D values by a factor 4. With the present version of our 2D code we are unable to predict in these cases where the energy is absorbed. In the present version the power is evaluated by calculating $\underline{j} \cdot \underline{E}^*$ at the antenna. We shall be able to give a definite answer, once a local evaluation of the energy flux within the plasma is implemented in ERATO.

7. CONCLUSIONS

We have shown that toroidal plasmas with circular cross-section may be heated right inside by choosing an antenna structure and a pump frequency such that a collective mode is excited. For Solovév equilibria of aspect ratios as small as 3 we do not find any toroidal effects on the absorbed power when the resonant surface is placed inside half the plasma radius. We have demonstrated the suitability of a 1D model in this case. Even with toroidicity the power is absorbed in the interior of the plasma contrary to certain pessimistic conjectures which have been made in the past. On the other hand we found that toroidicity considerably shifts the location of the resonant surfaces towards the plasma centre and also that it increases the reactive energy contained in the plasma. The resulting Q-value is acceptable from the experimental point of view. The increased reactive energy may be explained by the excitation of modes with high m-numbers near the plasma edge which could have a deleterious effect on the plasma transport properties in this region. On the Wisconsin stellarator⁴ enhanced transport has in fact been observed and ascribed to the formation of magnetic islands in some resonant regions. It might be that similar phenomena will happen in Tokamaks.⁶ Unfortunately, it is impossible to anticipate an answer on the basis of our ideal MHD model because the amplitudes of the excited fields are entirely determined by the artificial damping rate used in the model. The inclusion of real resistivity will improve this situation to some extent. A complete description of Alfvén wave heating would also demand the inclusion of kinetic effects.¹⁴

ACKNOWLEDGEMENTS

It is a pleasure to thank R. Keller and A. Pochelon for many fruitful discussions. Also we would like to thank A. Cheetham for reading the manuscript.

This work has been supported by the Swiss National Science Foundation, the Ecole Polytechnique Fédérale de Lausanne and by Euratom.

REFERENCES

- {1} Grossmann, W., Tataronis, J., Z. Phys. 261 (1973) 217
- {2} Hasegawa, A., Chen, L., Phys. Rev. Lett. 32 (1974) 454
- {3} Keller, R., Pochelon, A., Nucl. Fus. 18 (1978) 1051
- {4} Shohet, J.L. et al., Plasma Physics and Contr. Nucl. Fusion Research 1978 (proc. 7th Int. Conf., Innsbruck, 1978) IAEA, Vienna (1979), Vol. II, p. 569
- {5} Kalinichenko, S.S., et al., 9th Europ. Conf. Contr. Fusion and Plasma Phys., Oxford 1979, paper AP9
- {6} Cheetham, A.D., et al., "The TCA Tokamak", Lausanne Report, LRP 162/80, January 1980
- {7} Chen, L., Hasegawa, A., Phys. Fluids 17 (1974) 1399
- {8} Appert K., et al., 8th Int. Conf. Plasma Phys. and Contr. Nucl. Fusion Research, Bruxelles, 1980, paper IAEA-CN-38/D-1-1
- {9} Solovev, L.S., Sov. Phys.-JETP 26 (1968) 400
- {10} Berger, D., et al., ZAMP 31 (1980) 113
- {11} Appert, K., et al., Computer Phys. Comm. 10 (1975) 11

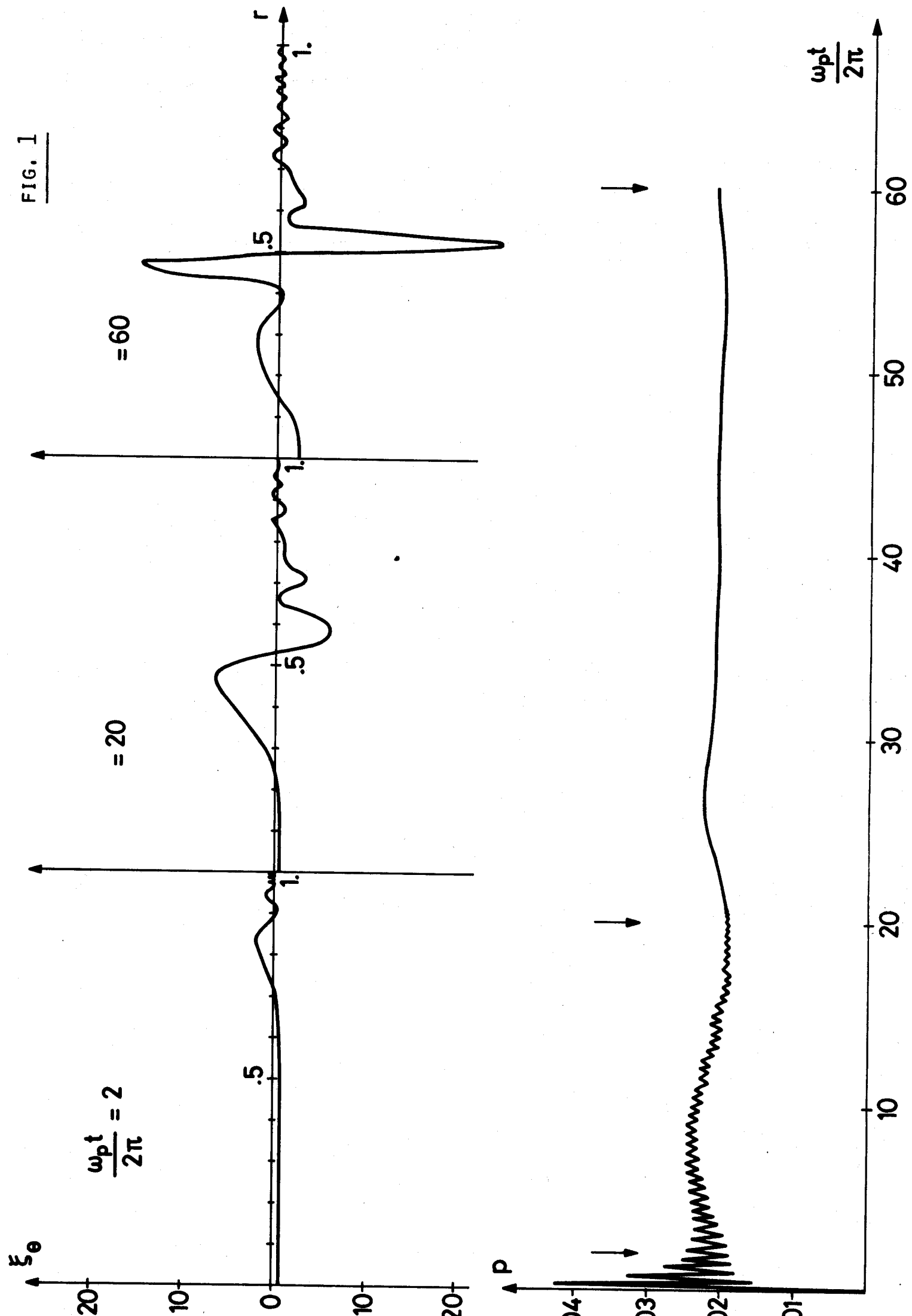
REFERENCES (cont'd)

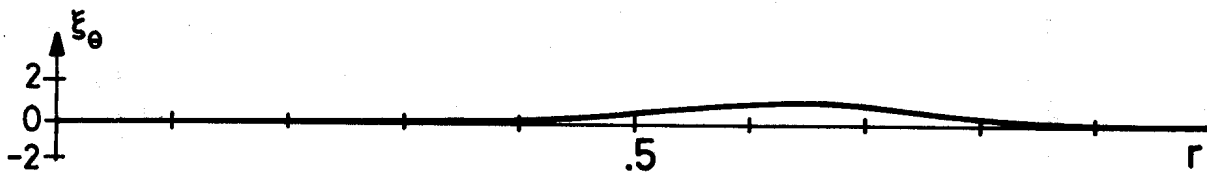
- {12} Gruber, R., et al., accepted for publication in Computer Phys. Comm.
- {13} Ginzburg, V.L., "Propagation of Electromagnetic Waves in Plasma", Gordon and Breach, New York (1961) p. 500
- {14} Hasegawa, A., Chen, L., Phys. Fluids 19 (1976) 1924

FIGURE CAPTIONS

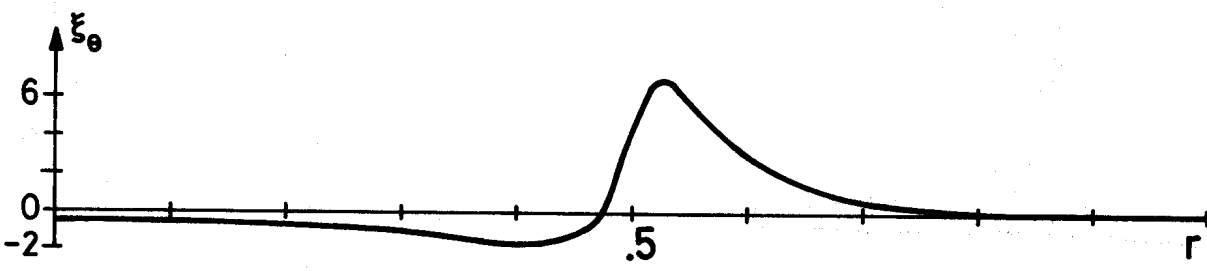
- Fig. 1 Time evolution of poloidal displacement and absorbed power.
- Fig. 2 Stationary response of poloidal displacement and absorbed power for different artificial damping rates versus radius.
- Fig. 3 Absorbed power versus artificial damping rate.
- Fig. 4a Stationary response of plasma displacement in poloidal plane
Fig. 4b for $\nu = 0.03$ and $\nu = 0.3$.
- Fig. 5 Fourier amplitudes near resonant surface for $a/R = 0.275$.
- Fig. 6 Fourier amplitudes at resonant surface versus inverse aspect ratio.
- Fig. 7 Local Alfvén frequencies versus radius in 1D model for $n = 5$.
- Fig. 8 Dominant Fourier amplitudes versus radial coordinate s in 2D model.
- Fig. 9 Absorbed power and Q-value versus inverse aspect ratio according to 1D and 2D models. Resonance with collective mode is approached for high a/R .
- Fig. 10 Absorbed power and Q-value versus toroidal wave number for $a/R = 0.275$ according to 1D and 2D models.
- Fig. 11 Absorbed power versus pump frequency. Location of resonant surfaces is indicated by r_s (1D) and s_r (2D).

FIG. 1

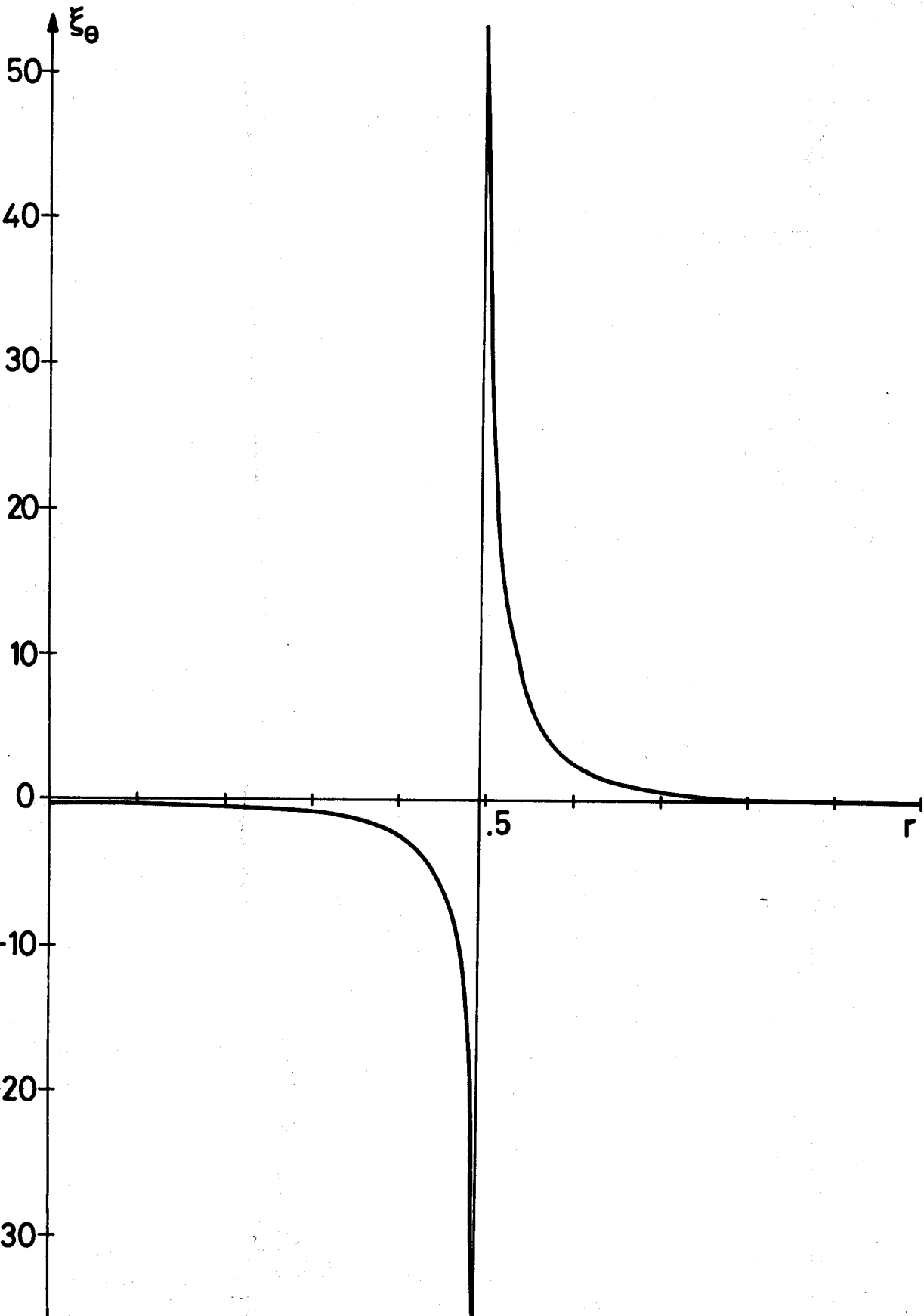




$v/\omega_p = .1$
 $\rho = .0199$



$v/\omega_p = .01$
 $\rho = .0212$



$v/\omega_p = .0007$
 $\rho = .0214$

FIG. 2

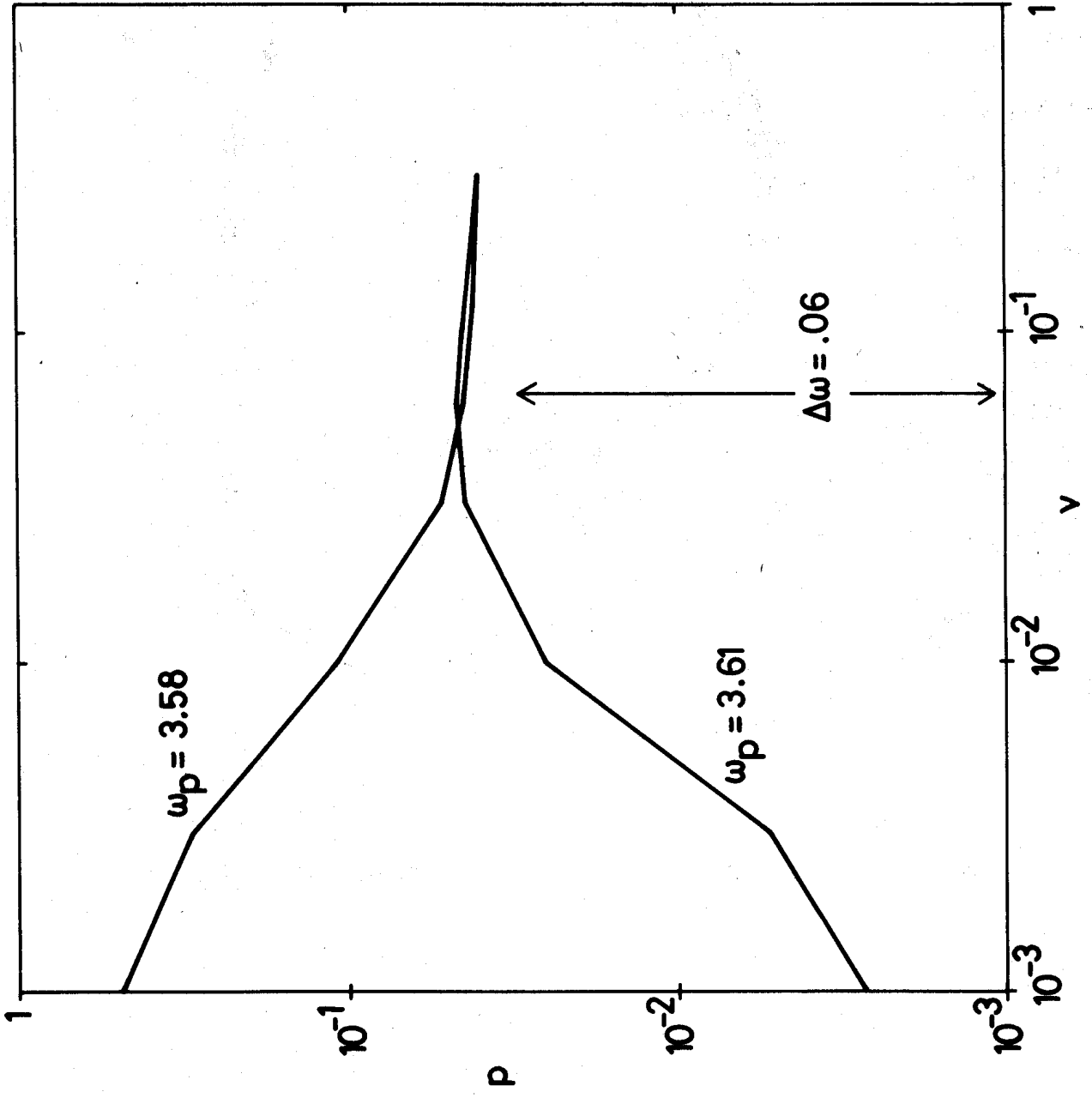
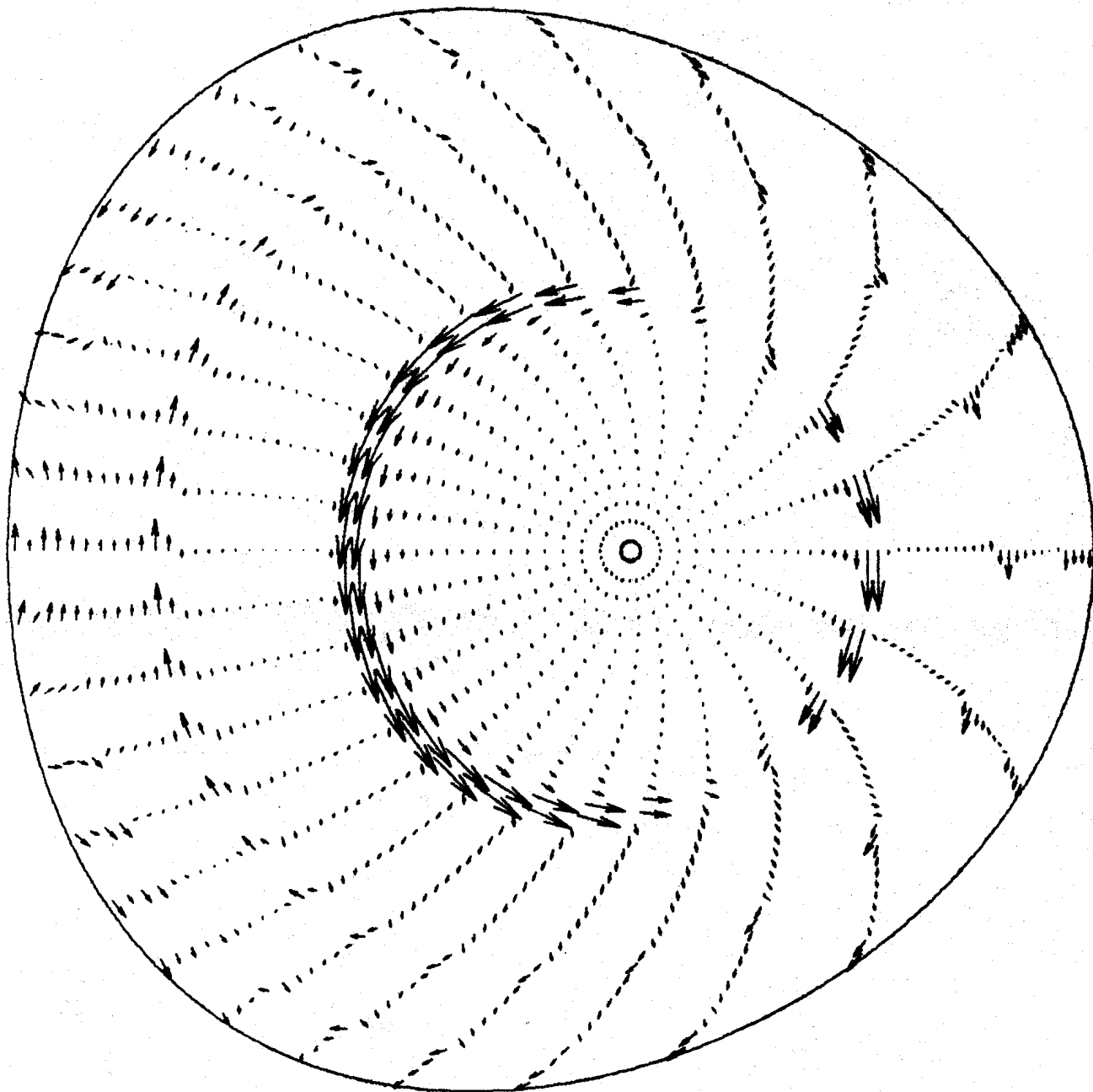


FIG. 3

FIG. 4A

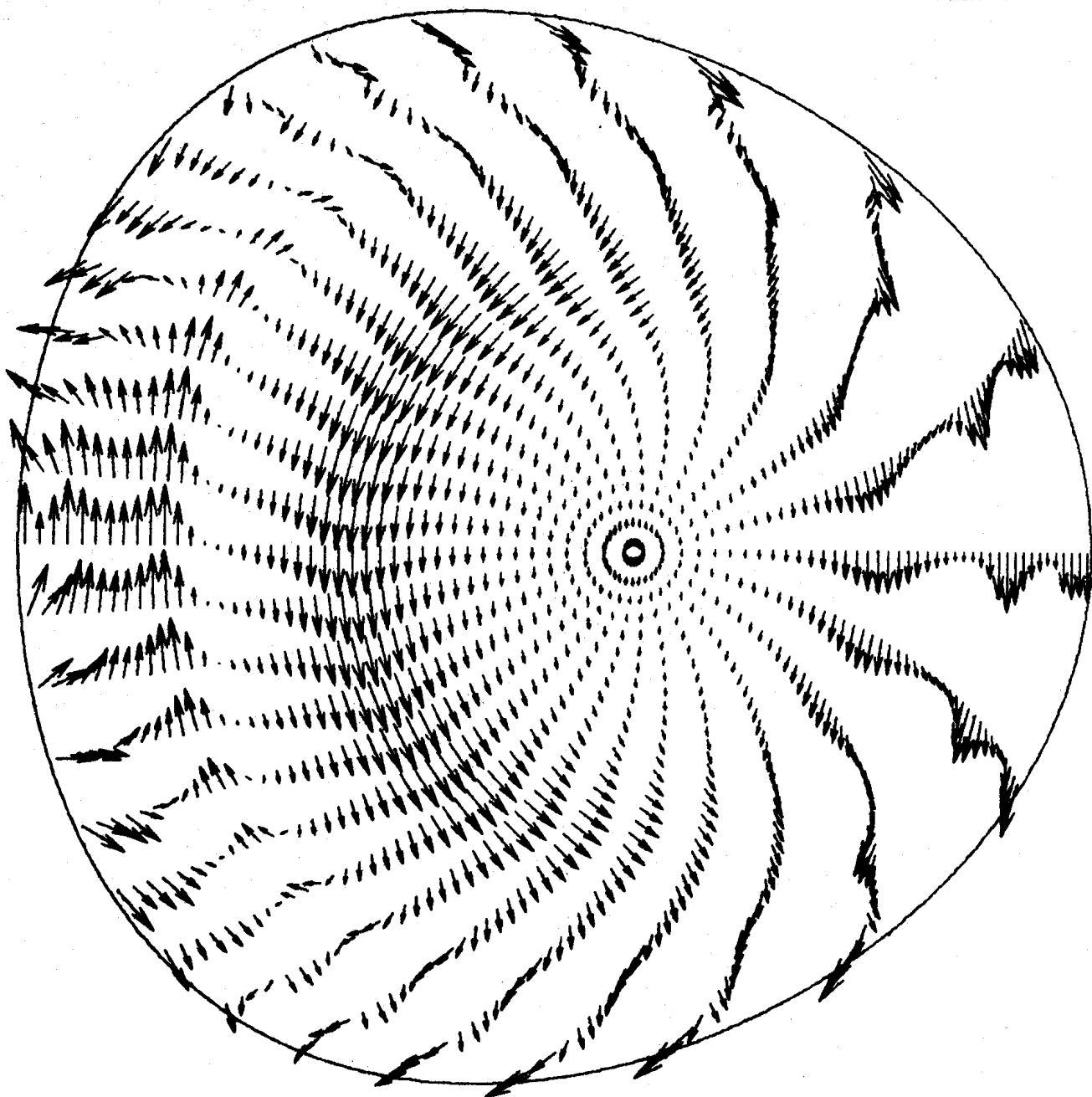


PHI = 0

CRPP EPF - LAUSANNE

"ERATO" 19/06/80

FIG. 4B



PHI = 0

CRPP EPF - LAUSANNE

"ERATO" 19/06/80

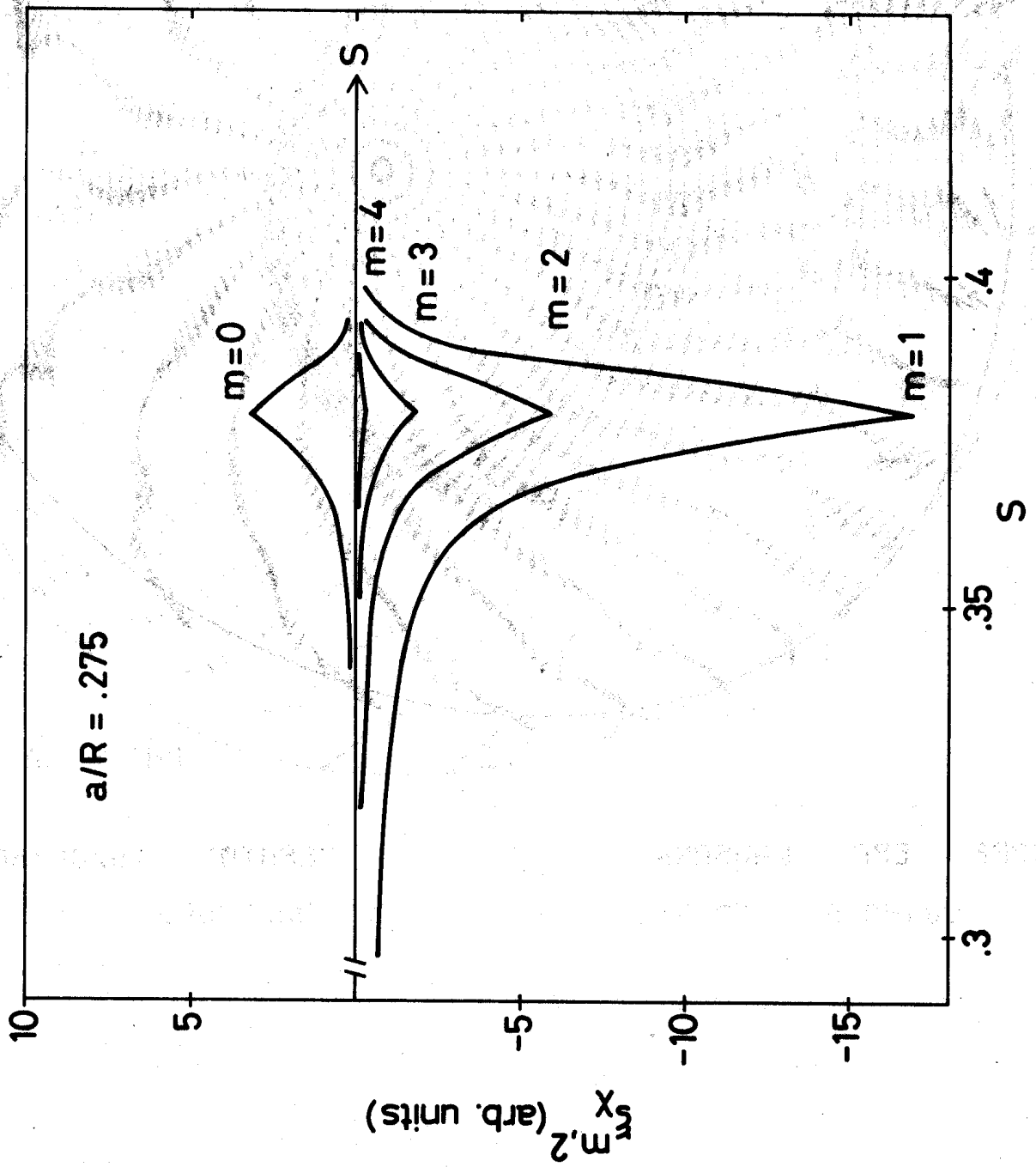


FIG. 5

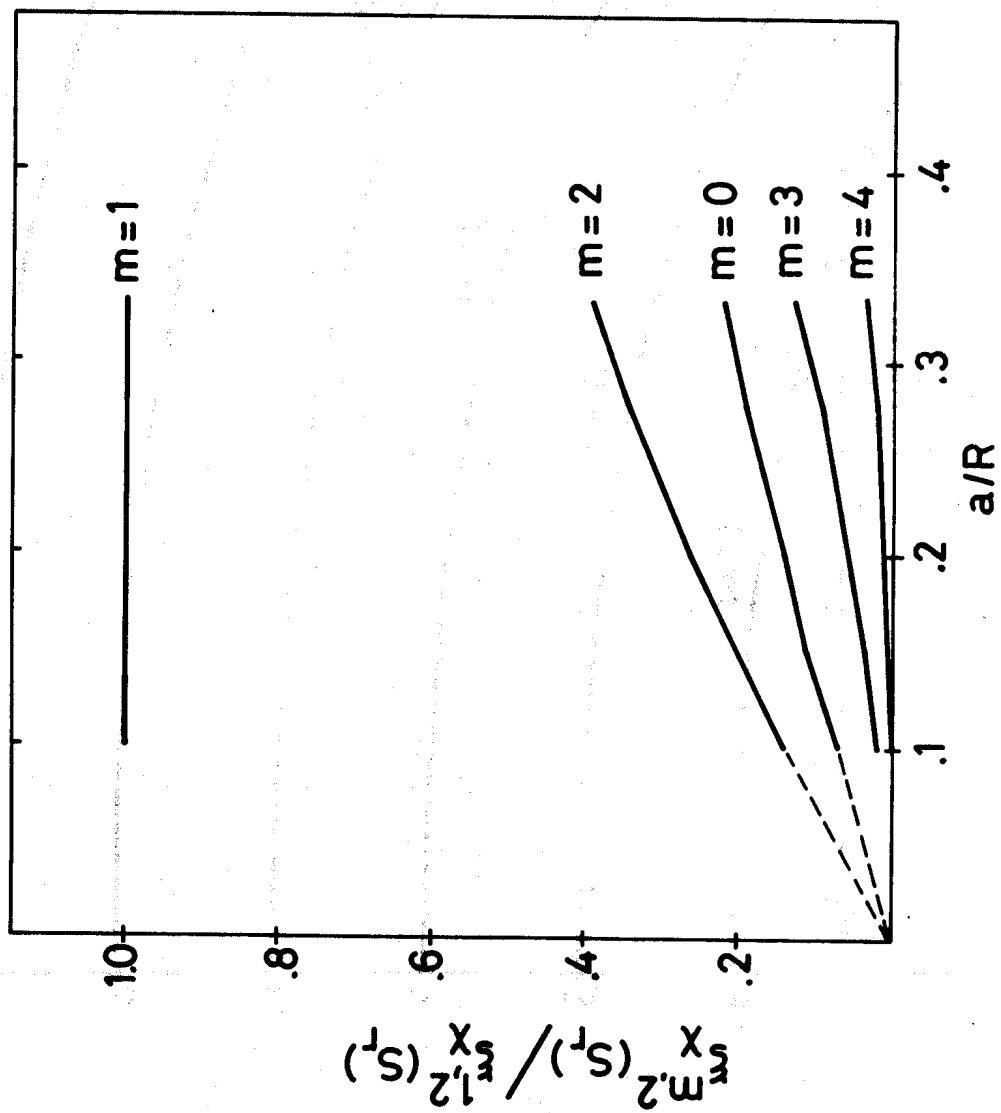


FIG. 6

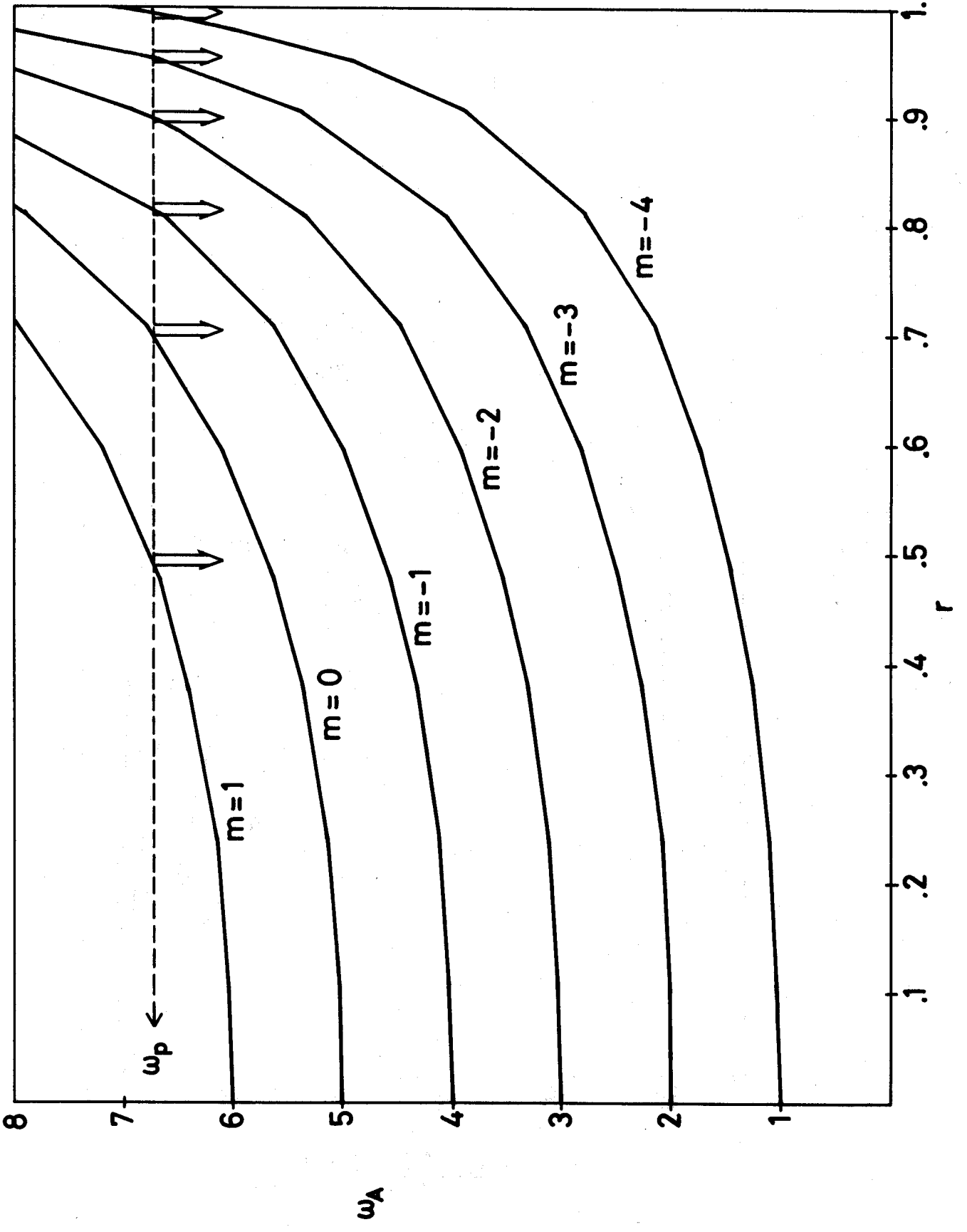


FIG. 7

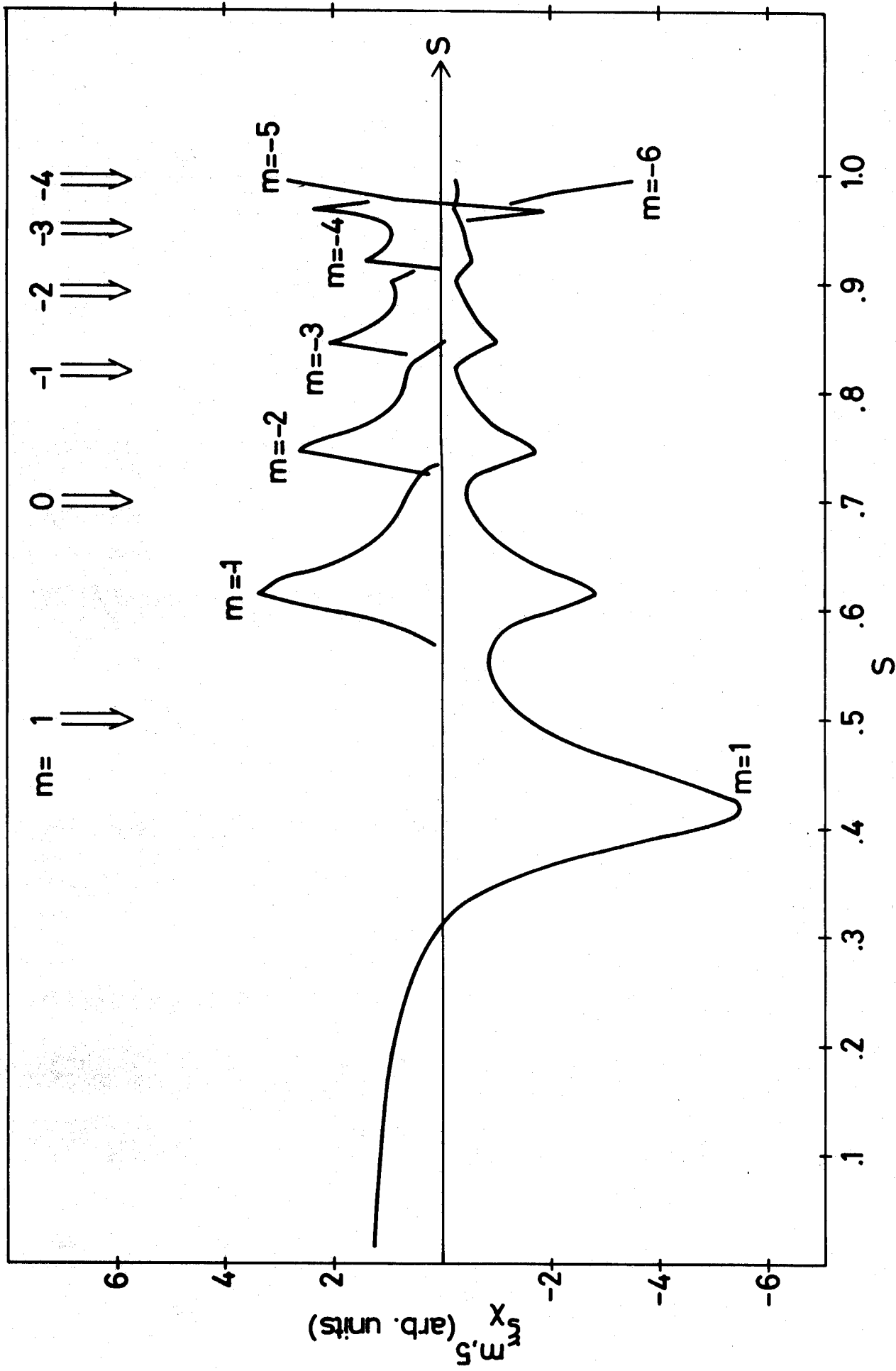


FIG. 8

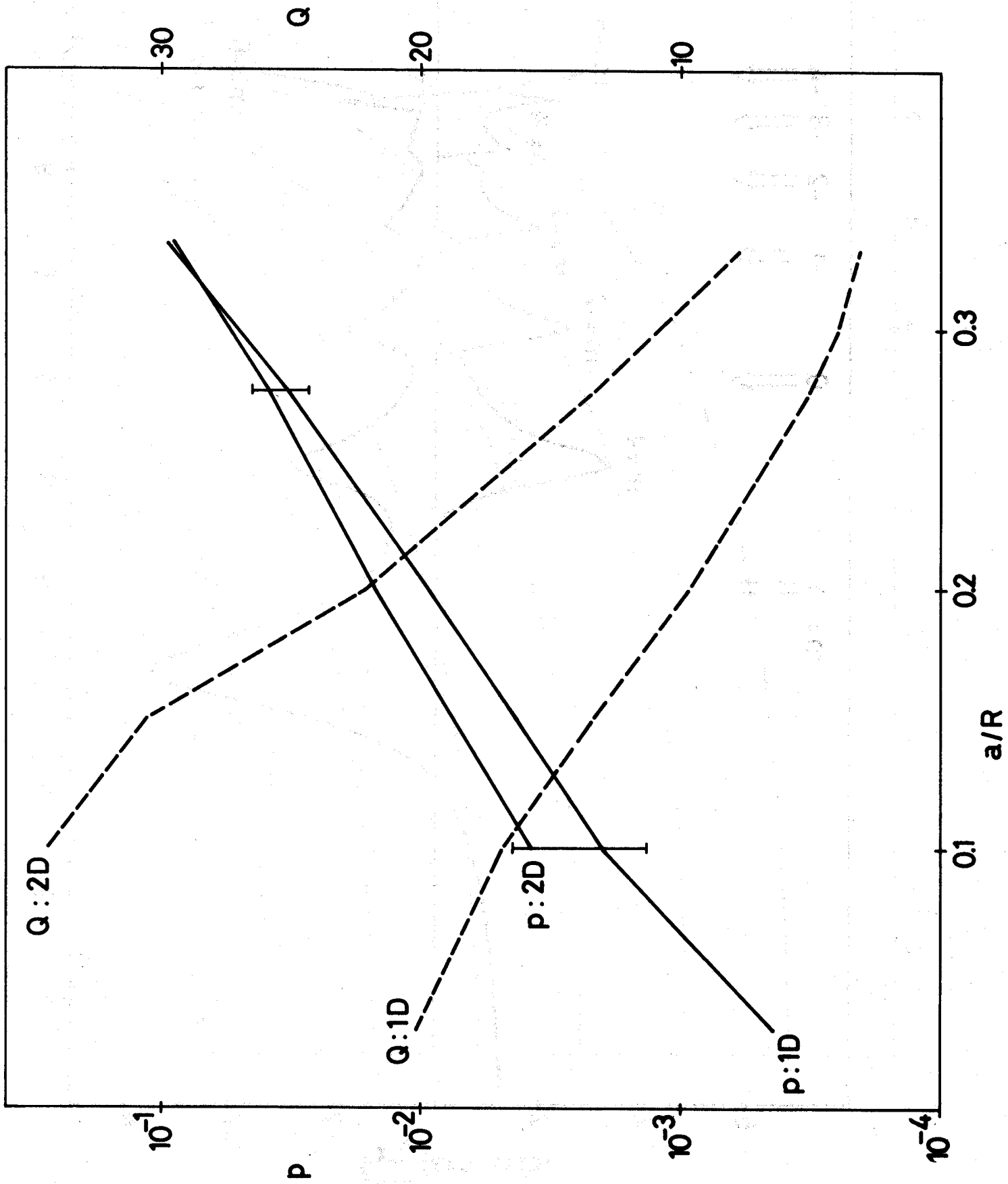


FIG. 9

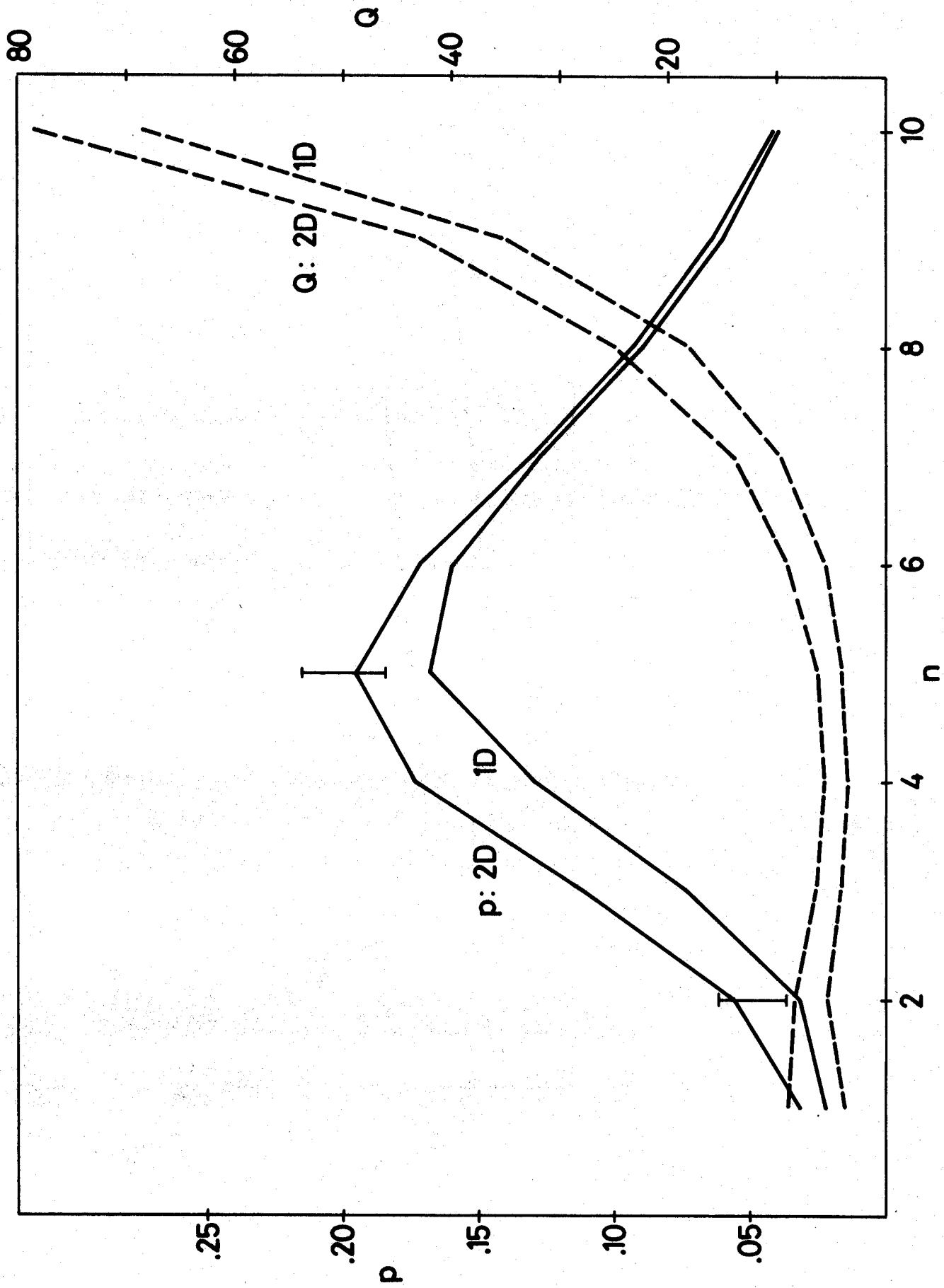


FIG. 10

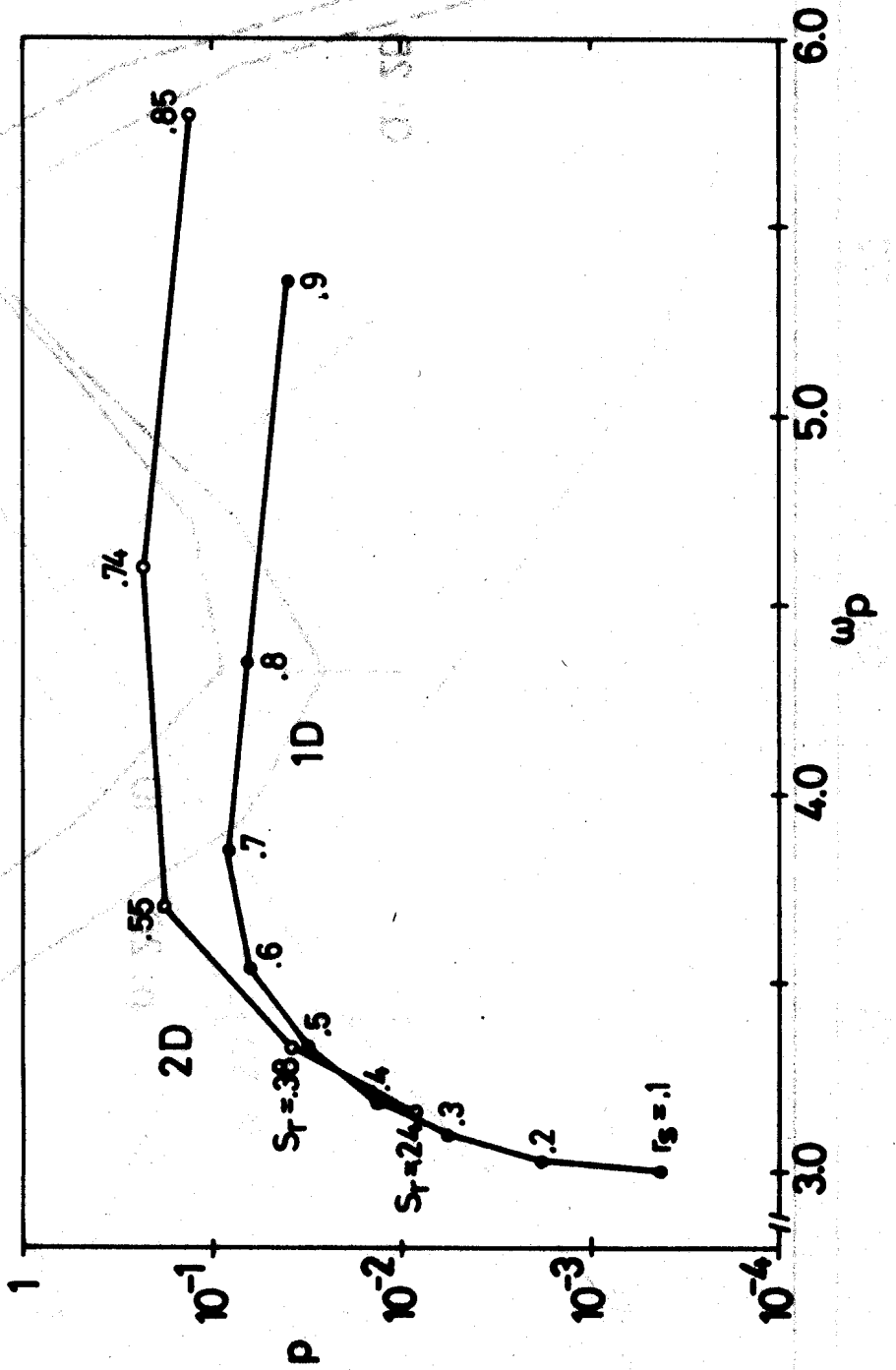


FIG. 11